4

Zn substituted Fe$_3$C (Zn$_x$Fe$_{3-x}$C; $0 \leq x \leq 1$)

4.1 Introduction

In previous chapter, it has been emphasized that Fe$_3$C particles can be produced by sol-gel technique and their physical as well as biocompatible properties were analyzed. This chapter discusses the effect of Zn substitution in Fe$_3$C. These samples were also prepared by same technique. The structural and magnetic properties of Zn$_x$Fe$_{3-x}$C ($0.1 \leq x \leq 1$) nanoparticles were analyzed using X-ray diffraction, electron diffraction and magnetic properties measurement system respectively. The modification of the morphology of the MNP$_S$ with increased substitutions of Zn was analyzed by Transmission electron microscope. The as prepared samples contain Fe, Zn and C which was confirmed by X-ray photoelectron spectroscopy. The heating abilities of the ferrofluids, prepared using F127 polymer were measured and subsequently their specific loss power (SLP), as well as intrinsic loss power (ILP) values were evaluated. Moreover, cytotoxicity of these MNP$_S$ was examined with human lung adenocarcinoma (A549) cells using SRB assay.

4.2 Results and discussion

4.2.1 Structural analysis by X-ray diffraction

The structural analysis of as-synthesized $Zn_xFe_{3-x}C$ ($0 \leq x \leq 1$) MNPs was accomplished using XRD. The Rietveld refinement of these diffraction patterns was done using Fullprof software to analyze the changes in the structural parameters with increasing substitution of Zn. The peaks of the patterns were found to match well with the standard data of Fe_3C (Cohenite i.e. JCPDS file # 65-2413) for all the samples (Fig. 4.1). The parameters obtained after Rietveld refinement are presented in Table 4.1. The fitted data (Table 4.1) suggest that Zn atoms have replaced iron atoms from the unit cell even at a lower concentration ($x = 0.1$). This can be accomplished to their equivalent atomic radii (e.g. Zn = 1.33 Å and Fe = 1.24 Å). The phase diagram of Fe-Zn suggests that Zn has around 42 at.% solubility in Fe at 782 ºC but decreases down to only a few at% at ambient temperature [79]. Thus, it was expected to achieve a single phase for $Zn_{0.1}Fe_{2.9}C$ sample. Though, these two elements form several intermetallic compounds but the samples ($Zn_xFe_{3-x}C$) were found to be monophasic up to $x = 1$. Further, there was no evidence of other Fe-Zn based intermetallic compounds from XRD patterns of the samples (Fig. 4.1). It indicates that Zn atoms could substitute Fe in Fe_3C up to the range cited in this work i.e. around 33 at.%. It has been described in the literature that Fe has two different positions in Fe_3C [Fe1 (*8d*) and Fe2 (*4c*) Wyckoff positions] and for all the samples (i.e. $x \leq 1$), Zn atoms replaced Fe atoms from both the sites (Table 4.1). The variations in the lattice parameter and the unit cell volume for the samples are shown in Table 4.1 and Fig. 4.2 respectively. These variations were observed to be random with increased content of Zn in Fe_3C. However, the lattice parameter "a" and "c" as well as

"cells volume" had a similar trend with an enhanced concentration of Zn (Fig. 4.2). In contrast, the lattice parameter "b" had reverse trend than these parameters (Fig. 4.2).
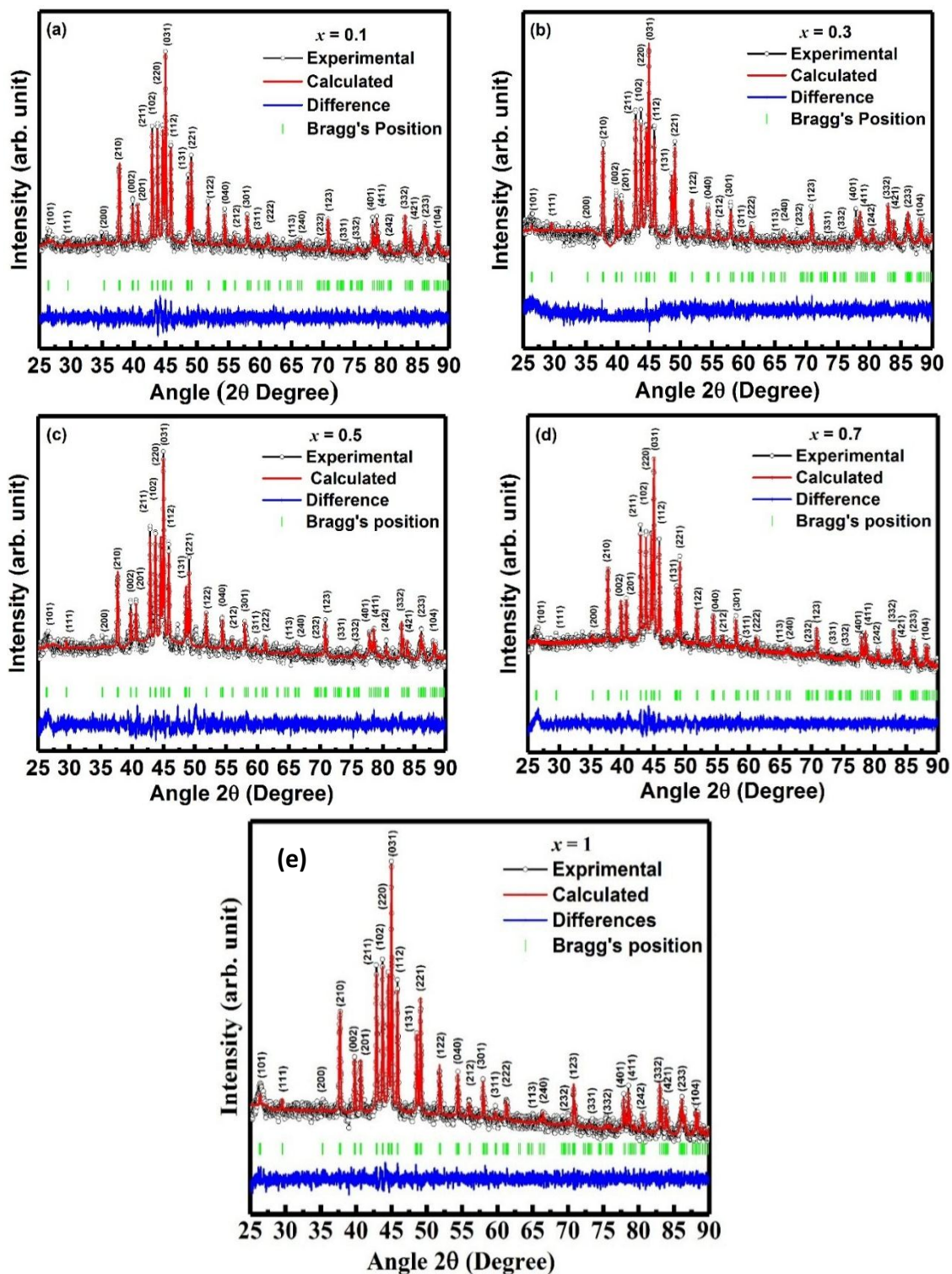

Figure 4.1: Rietveld refined diffraction patterns of the $Zn_xFe_{3-x}C$ (x = 0.1, 0.3, 0.5, 0.7 and 1) system.

The synthesis of $Zn_xFe_{3-x}C$ phase was possible by the sol-gel route and subsequent calcination at 700 °C in an N_2 atmosphere. The mechanism involved in the formation of iron carbide phase has been discussed in detail in chapter 3.

Table 4.1: Summary of the Rietveld refined structural parameters of the orthorhombic $Zn_xFe_{3-x}C$ $(0.1 \leq x \leq 1)$ nanoparticles.

| Sample Parameters	x = 0.1	x = 0.3	x = 0.5	x = 0.7	x = 1
Space group and crystal structure	Pnma 62, Orthorhombic				
Lattice parameters a,b,c	5.0921	5.0918	5.0922	5.0915	5.0915
	6.7432	6.7435	6.7431	6.7431	6.7431
	4.528	4.5280	4.5284	4.5277	4.5275
$\alpha = \beta = \gamma$	90				
Unit cell Volume Å³	155.4786	155.4746	155.4927	155.4498	155.4398
Atomic position x, y, z Fe1 = Zn1	0.18058	0.17675	0.17868	0.17959	0.18018
	0.06492	0.06515	0.06434	0.6563	0.06586
	0.3379	0.34108	0.34003	0.33072	0.3314
Atomic position x, y, z Fe2 = Zn2	0.03497	0.87676	0.03359	0.03487	0.03853
	0.25	0.25	0.25	0.25	0.25
	0.8384	0.4159	0.83544	0.84542	0.84016
Atomic position x, y, z C1	0.88015	0.8767	0.9024	0.87236	0.88381
	0.25	0.25	0.25	0.25	0.25
	0.44497	0.4159	0.46089	0.43379	0.44746
Quality fitting factors (χ^2,R_p,R_w)	1.12	1.4	1.19	1.29	1.3
	9.56	16.6	6.74	11.1	6.53
	9.46	14.5	4.52	10.5	6.97
Atomic Occupancy site					
Fe1	1.9635	1.90106	1.91726	1.71134	1.7263
Fe2	0.9365	0.79894	0.58274	0.58866	0.2737
Zn1	0.0699	0.20005	0.30264	0.49714	0.68657
Zn2	0.0301	0.09995	0.19736	0.20286	0.31343
C	1	1	1	1	1
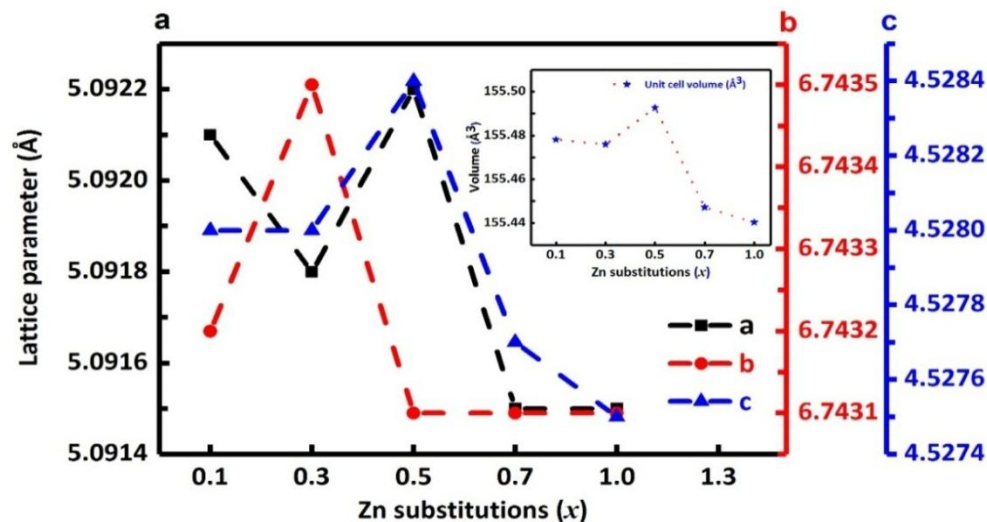
Figure 4.2: Variation in the lattice parameter for $Zn_xFe_{3-x}C$ ($0.1 \leq x \leq 1$) system and inset showing decrease in unit cell volume

4.2.2 Morphological analysis using TEM

The TEM micrograph for the sample $x = 0.1$, is shown in Fig.4.3. The morphology of the sample was nearly spherical which is presented in Fig. 4.3 (a). The electron diffraction pattern for this sample is shown in Fig 4.3 (b) which displays a ring pattern indicating polycrystalline behavior for the sample. The SAED pattern was indexed with the help of eRing software (Fig. 4.3 b). The d spacing values for this pattern were 3.02, 2.54, 2.06, 1.76, 1.63, 1.51, and 1.29 Å which correspond to the planes (111), (200), (102), (122), (212), (222) and (051) respectively for Fe_3C phase. The HR-TEM micrograph represents the fringe width ~ 0.238 nm which corresponds to the (121) plane of Fe_3C (Fig. 4.3 c). The SAED pattern further supported the presence of any other phases in the sample which also justified XRD results. In addition, in the inset of Fig. 4.3 (c), a boundary of few nanometer thicknesses (~ 4 nm) was also observed surrounding to the particles ($x = 0.1$) and it may be amorphous carbon. The formation of

carbon coatings over pure as well as Co substituted Fe_3C are also reported in earlier literature [25].
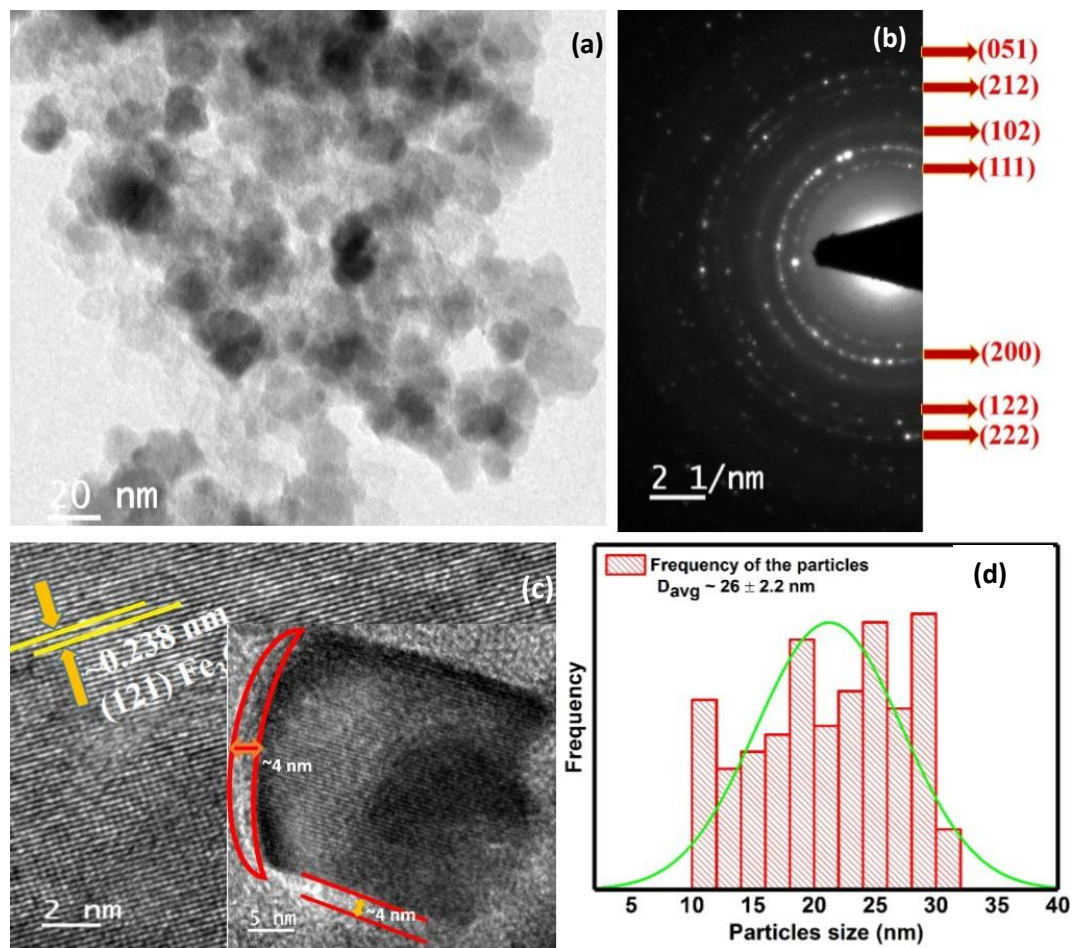

Figure 4.3: Transmission electron micrograph for sample $x = 0.1$ a) bright field micrograph, b) SAED pattern c) HR-TEM micrograph and d) histogram of the particles.

The size distribution for $x = 0.1$ sample was estimated from 200 particles using ImageJ software, and the histogram is shown as Fig. 4.3 (d). The size of the nanoparticles was determined to be in the range of 10 – 32 nm and the average particle size was ∼ 26 ± 2 nm.

The TEM micrograph for the sample $x = 1$ is shown in Fig. 4.4 (a). It contains both spheroidal and cuboidal shaped particles. Thus the morphology of these particles was different from that of $x = 0.1$ sample which contains only spheroidal particles (Fig. 4.4 a). The formation of cuboidal shape was also observed for Mn- or Co-doped Fe_3C at their higher contents [25]. It has been claimed that the dopants like Mn, Co, Ni or Zn distort the lattice of Fe_3C and facilitate the formation of cuboidal shape at higher concentration [25, 40].
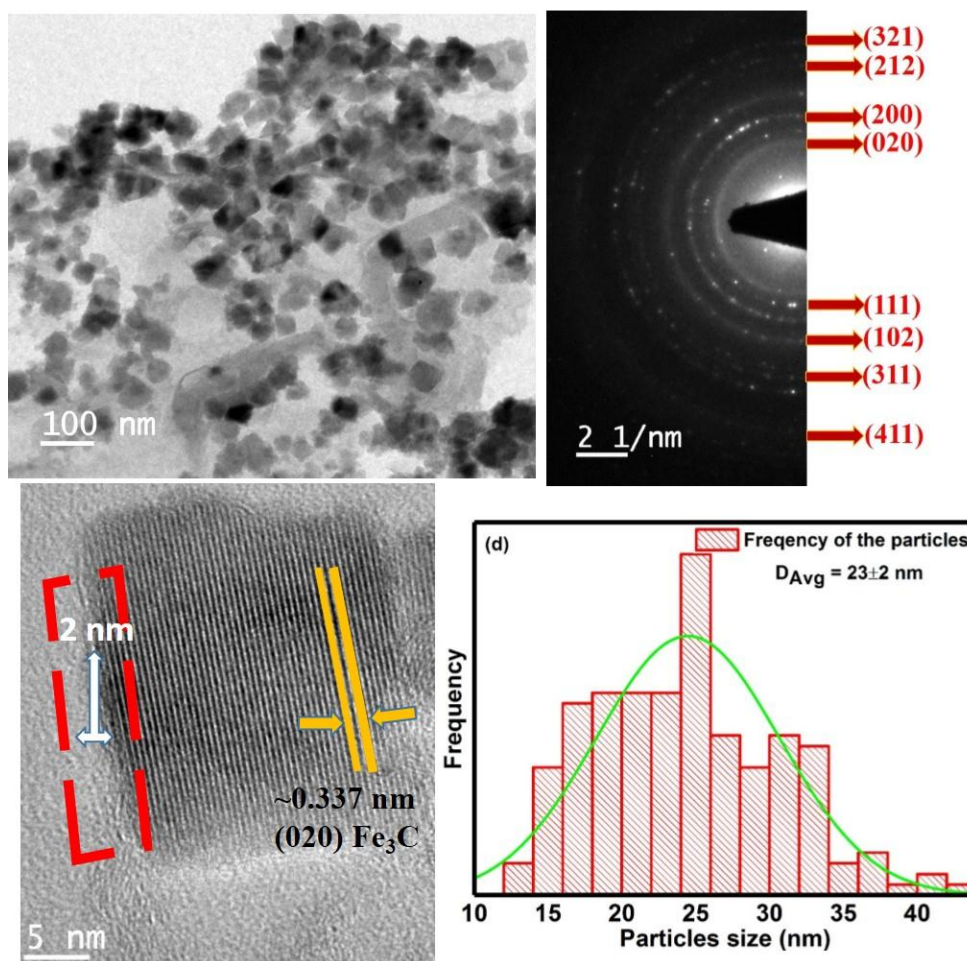

Figure 4.4: Transmission electron micrograph for sample $x = 1$ a) bright field image, b) SAED pattern, c) HR-TEM micrograph and d) histogram of the particles.

The SAED pattern for this sample was indexed with the help of eRing software, and the d spacing values were obtained to be 3.37, 3.02, 2.5, 2.06, 1.639, 1.54, 1.44, and 1.2 Å (Fig. 4.4 b). These values match with the planes (020), (111), (200), (102), (212), (311), (321) and (411) respectively (Fig. 4.4 b) for Fe_3C phase. The fringe width from the HR-TEM micrograph was also estimated by ImageJ software and the obtained value (~ 0.337 nm) designates the (020) plane of Fe_3C phase (Fig. 4.4 c). This also confirms the XRD findings that Zn substitutes Fe in Fe_3C up to a large extent (~ 33 at. %). The micrograph further suggests the presence of a carbon layer of thickness around 2 nm over the sample (Fig. 4.4 c). Nevertheless, the thickness of the coating was lesser than that of pure Fe_3C or $x = 0.1$ sample which could be ascribed to the reduced graphitization at a higher concentration of Zn. With the help of ImageJ software, the particle size distribution was estimated for this sample after considering around 200 particles. The histogram suggests that the particle size was between 12-45 nm and the average particle size was ~ 23 ± 2 nm (Fig. 4.4 d). There was no significant change in the particle size with increased Zn content.

4.2.4 XPS Analysis

X-ray photoelectron spectroscopy was employed for the identification of oxidation states for Fe, C, Zn and O elements over the surface of the sample. Fig. 4.5 shows deconvoluted XPS spectra of Fe 2p, C 1s, Zn 2p, and O 1s for $Zn_xFe_{3-x}C$ ($x = 0.3$) sample. As shown in Fig. 4.6 (a), the high-resolution spectrum of Fe 2p can be deconvoluted into three peaks at 711.79, 719.53 and 725.39 eV. The peaks at 711.79 and 725.39 eV can be ascribed to the Fe $2p_{3/2}$ and Fe $2p_{1/2}$ respectively which represent the Fe atomic state.

The satellite peak at 719.53 eV could be ascribed to the Fe 2p3/2 for Fe^{3+} state due to oxidation at the surface i.e. Fe_2O_3 phase. Since the oxide phase does not contain Fe^{2+} ions and hence its satellite peak was absent. The spectrum of C 1s after deconvolution is shown in Fig. 4.6 (b). The observed three peaks at 284.9, 285.73 and 288.9 represent the C-C, C-O-C and O-C=O bonds respectively. The C-C peak designates the bonding between metal-carbon whereas the other two peaks are for its bonding with oxygen. Such bonding could be due to the interaction of oxygen with carbon which exists as coating over the surface of Fe_3C (Figs. 4.3 c and 4.4 c).
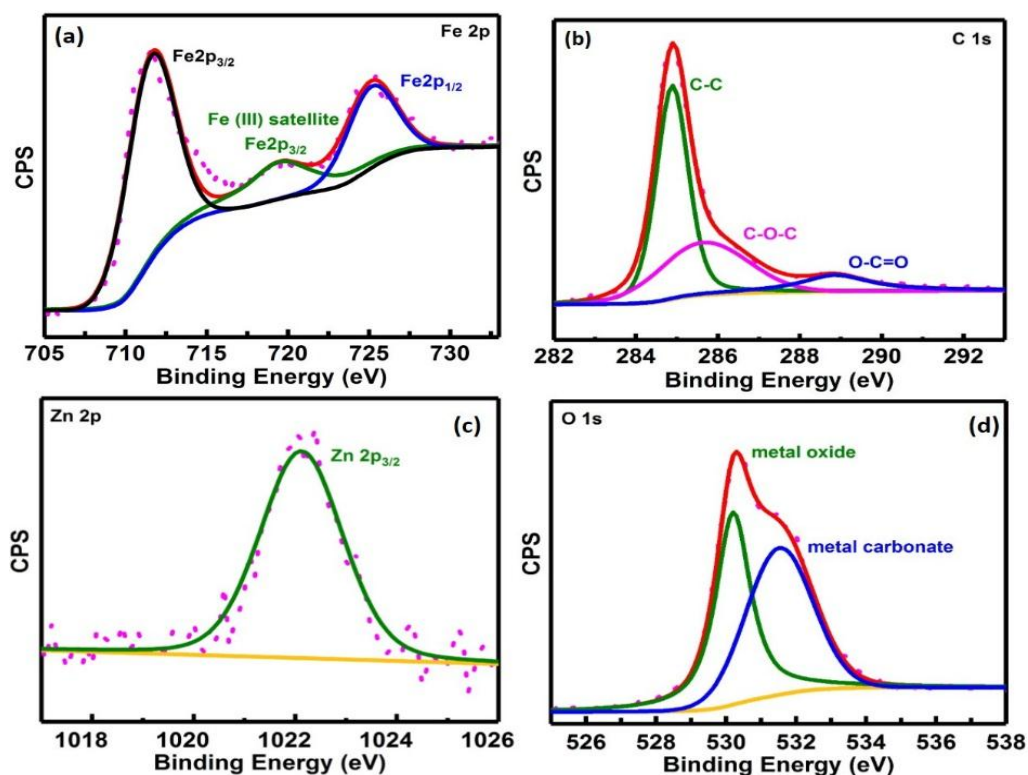

Figure 4.5: XPS spectra of sample $x = 0.3$ (a) Fe 2p core level spectra, (b) C 1s core level spectra, (c) Zn 2p and (d) O 1s.

.

The spectrum for Zn 2p is shown in Fig. 4.5 (c) and the peak at 1022 eV depicts the Zn 2p3/2. The O 1s spectrum had two peaks at 530.5 and 531.5 eV. The former can be ascribed to metal-oxygen bonding and the latter one to C-O bonding (Fig. 4.5 d).

4.2.5 Mössbauer spectroscopy

Mössbauer spectroscopy was used to analyze the purity level as well as the magnetic behavior of the $Zn_xFe_{3-x}C$ ($x = 0.1$ and 0.5) nanoparticles at 300 K (figure 4.6). The values of the magnetic hyperfine field (B_{hf}), quadruple splitting (QS, Δ), isomer shift (IS, δ), the line width (Γ), and relative area (R_A) are compiled in Table 4.2. The spectrum for $x = 0.1$ sample was fitted with one sextet (Zeeman splitting pattern) and a doublet (Fig 4.6 a). The B_{hf} value for the sextet was 20.91 T. As stated earlier, in Fe_3C, there are two sites for Fe and hence it has two sextets with B_{hf} values of 20.9 and 20.6 T. Since the difference in their B_{hf} values is less than 1% thus they sometimes overlap and appear as a single sextet [25]. Similar spectrum i.e. the presence of only one sextet was also observed for $Co_xFe_{3-x}C$ ($0 \leq x \leq 0.3$) samples. The presence of doublet ($\sim$ 8%) could be attributed to the paramagnetic component of the material existing due to submicroscopic dimension particles. The IS values for the two spectra were 0.205 and 0.283 mm/s which were higher than the bulk Fe_3C but lower than that for pure Fe_3C prepared by similar technique. Similarly, the QS values were 0.015 and 0.8293 mm/s for the sextet and doublet respectively.

The experimental spectrum for the sample $x = 0.5$ is shown in Fig. 4.6 (b) which was fitted with two sextets and one doublet. The B_{hf} values for the two sextets were 20.92 and 18.25 T respectively which represents the two different sites of Fe in Fe_3C.
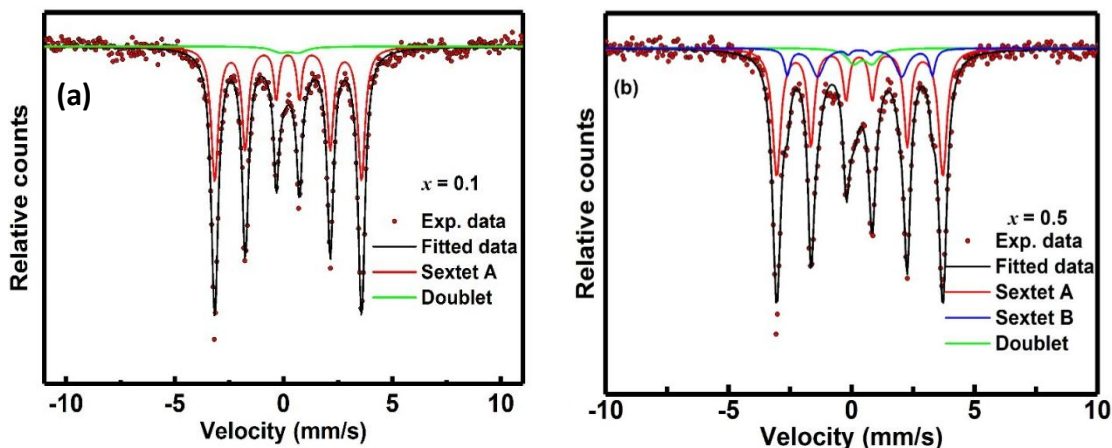
Figure 4.6: Mössbauer spectra of $Zn_xFe_{3-x}C$ for (a) $x = 0.1$ and (b) $x = 0.5$ samples.

The B_{hf} value for the first sextet was 0.02 T higher than that of bulk but it was around 2.35 T lesser than for the second sextet. The relatively more decrease in the B_{hf} value for the second sextet might be due to the presence of more content of Zn at this site. The composition (8%) of the doublet in the spectrum was similar to that for $x = 0.1$ sample (Table 4.2). The IS values for both the sites were nearly equal but higher than that of bulk Fe_3C.

Table 4.2: The hyperfine field values (B_{hf}), isomer shift (δ), quadruple splitting (Δ), Inner line width (Γ) and relative area (R_A) of Fe-sites for $Zn_xFe_{3-x}C$ ($x = 0.1$ and 0.5) derived from Mössbauer spectra, recorded at room temperature. Isomer shift values are relative to Fe metal foil ($\delta = 0.0$ mm/s).

Sample $Zn_xFe_{3-x}C$	Iron sites	Hyperfine field (H_f) T± 0.01	Isomer shift (δ) ± 0.01	Quadruple splitting, Δ (mm/s)± 0.01	Outerline width (Γ) mm/s	Relative area (%)	χ^2
	Sextet	20.91	0.20	0.02	0.38	92	
$x = 0.1$	Doublet	-	0.26	0.83	0.81	8	1.67
	Sextet A	20.92	0.21	0.02	0.41	77	
$x = 0.5$	Sextet B	18.25	0.22	0.01	0.343	15	1.41
	Doublet	-	0.31	0.75	0.66	8	

4.2.6 Magnetic characterization

The field dependent (±2 T) specific magnetization plots at 300 K for $Zn_xFe_{3-x}C$ ($0 \leq x \leq 1$) samples are presented in Fig. 4.7. The coercivity and remanence plots (near the origin) for all the samples are shown in the inset of this figure. The M_S values were found to be decreasing continuously from 58.4 to 53.3 Am^2/kg as the x value rose from 0.1 to 1.0 (Fig. 4.7 b). These values were lower than the value for unsubstituted Fe_3C nanoparticles (~ 62 Am^2/kg) as reported in our earlier work. The M_S values were also lesser than the published values for bulk Fe_3C which could be assigned to the smaller dimension of the present materials and the nonmagnetic carbon coating over the surface. However, the M_S values for these samples were higher than the transition element doped Fe_3C.

Further, there was only a slight decrement in the M_S values with increased amounts of Zn from $x = 0.1$ to $x = 1$. In contrast, the other substituents like Co or Mn or Ni have lowered the M_S values considerably which could be ascribed to the formation of antiferromagnetic coupling with Fe [25, 40]. On the other hand, Zn is diamagnetic and thus does not contribute to the reduction of the Ms value. Nevertheless, the observed continuous decrease in the Ms values with an enhanced concentration of Zn was solely due to the effective reduction of Fe in the materials (Fig. 4.7 b). The variation of coercivity (H_C) and remanence (M_r) values with increased Zn substitutions are shown in Fig. 4.7 (c). The H_C values were perceived to be decreasing and then increasing with Zn content and it rose from 14.4 mT for $x = 0.1$ to 15 mT for $x = 1$ sample (Fig. 4.7 c). This minor improvement in the coercivity may be accomplished to the shape anisotropy as

the particles transformed from spheroidal to cuboidal shape at higher Zn concentration (Figs. 4.3 a and 4.4 a).
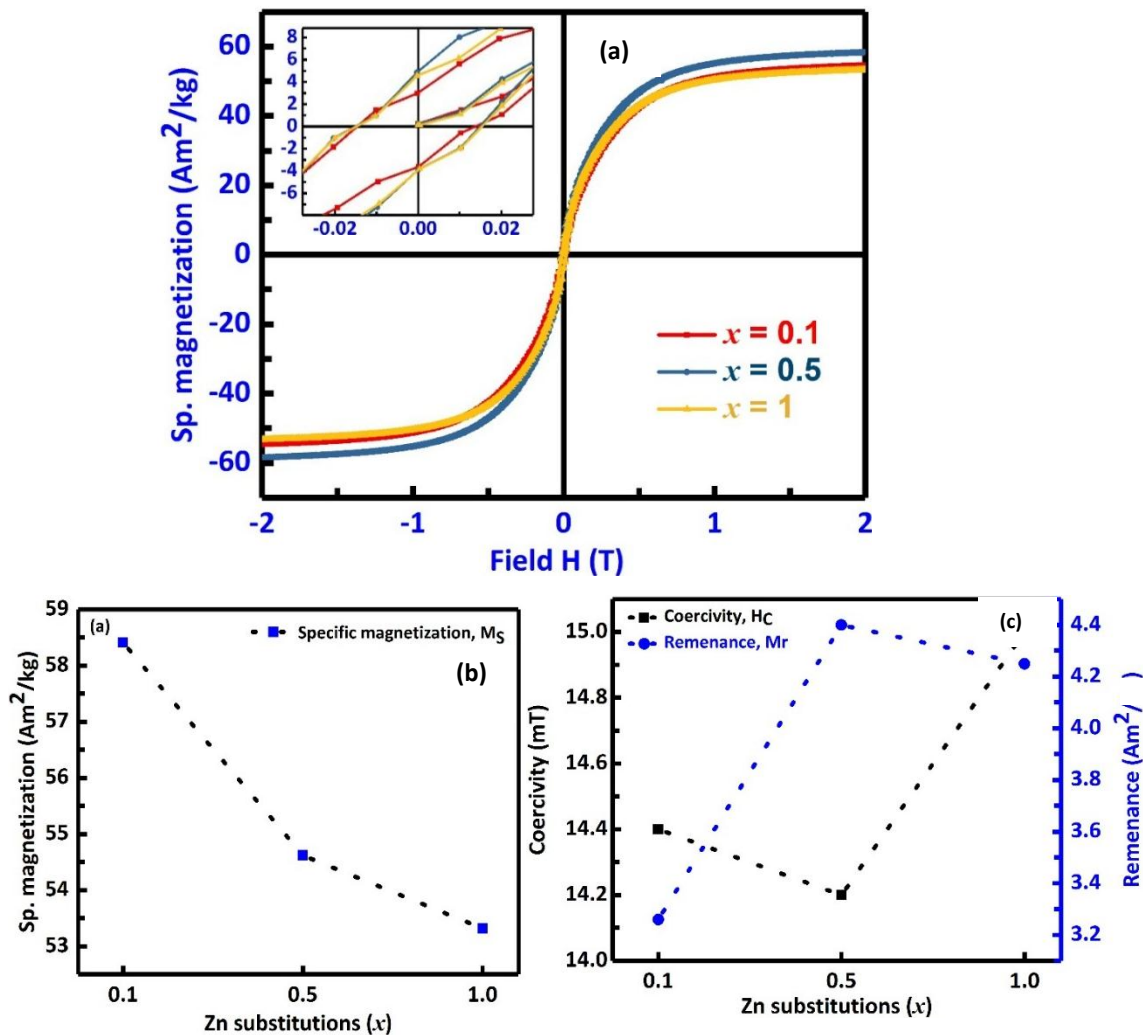

Figure 4.7: (a) M *vs.* H plots for all the samples $Zn_xFe_{3-x}C$ (x = 0.1, 0.5 and 1) (b) Variation in the saturation magnetization (M_S) values and (c) Coercivity (H_C), remanent (M_r) plots for samples $Zn_xFe_{3-x}C$ (x = 0.1, 0.5 and 1) with Zn substitutions.

The H_C values for the present samples were more than that for pure and Co-substituted Fe_3C but lesser than those of Mn- or Ni-substituted Fe_3C. The variations in the H_C values could be attributed to their shape and size. The particles of $Zn_xFe_{3-x}C$

samples were relatively larger than the particles of $Co_xFe_{3-x}C$ but smaller than that of Mn- or Ni-substituted Fe_3C. The M_r value for the sample $x = 0.1$ was 3.25 Am^2/kg which initially increased and then decreased with the rising proportion of Zn (Fig. 4.7 c). Similar to the H_C values, the M_r values for the present samples were higher than that of $Co_xFe_{3-x}C$ ($0 \leq x \leq 0.3$) samples due to relatively bigger sized particles.

4.2.7 Calorimetric measurements for magnetic fluids

The aqueous ferrofluids of $Zn_xFe_{3-x}C$ ($x = 0.1, 0.3, 0.5, 0.7$ and 1) samples were prepared using water soluble Pluronic polymer (F127) which acted as a stabilizer. The induction heating behavior for all the ferrofluids prepared using MNPs of concentration 10 mg/mL were observed initially at an AC field of 25 mT, 112 kHz (Fig. 4.8 a). All the ferrofluids have shown a continuous rise in temperature during this experiment. However, the time needed to reach therapeutic temperature of 42 ºC was 1018, 722, 195, 135 and 674 s for the samples $x = 0.1, 0.3, 0.5, 0.7$ and 1 respectively. It has been observed that the sample $x = 0.7$, was taking least time as compared to the other samples though it had relatively lower M_S value than $x \leq 0.5$ samples (Fig. 4.8 b). Likewise, all the ferrofluids were exposed to another AC magnetic field (24 mT, 543 kHz) and the data are shown in Fig. 4.8 (b). At this field also, continuous rise in temperature was marked for each sample. The essential therapeutic temperature for $x = 0.1, 0.3, 0.5, 0.7$ and 1 samples was achieved after exposure to the field for 502, 381, 345, 228 and 605 seconds respectively (Fig. 4.8 b). The observations suggest that the duration of exposure to magnetic fields to achieve therapeutic temperature diminished with increased concentration of Zn and it was least for the sample $x = 0.7$ (Figs. 4.8 a and b). Later, this

duration has increased and it was found to be maximum for the ferrofluids of sample x = 1, at both the fields. Thus, the samples in AC magnetic fields displayed contradictory behavior than the DC field as the M_S values continuously decreased with increased Zn content in Fe$_3$C (Figs. 4.8 a and b).
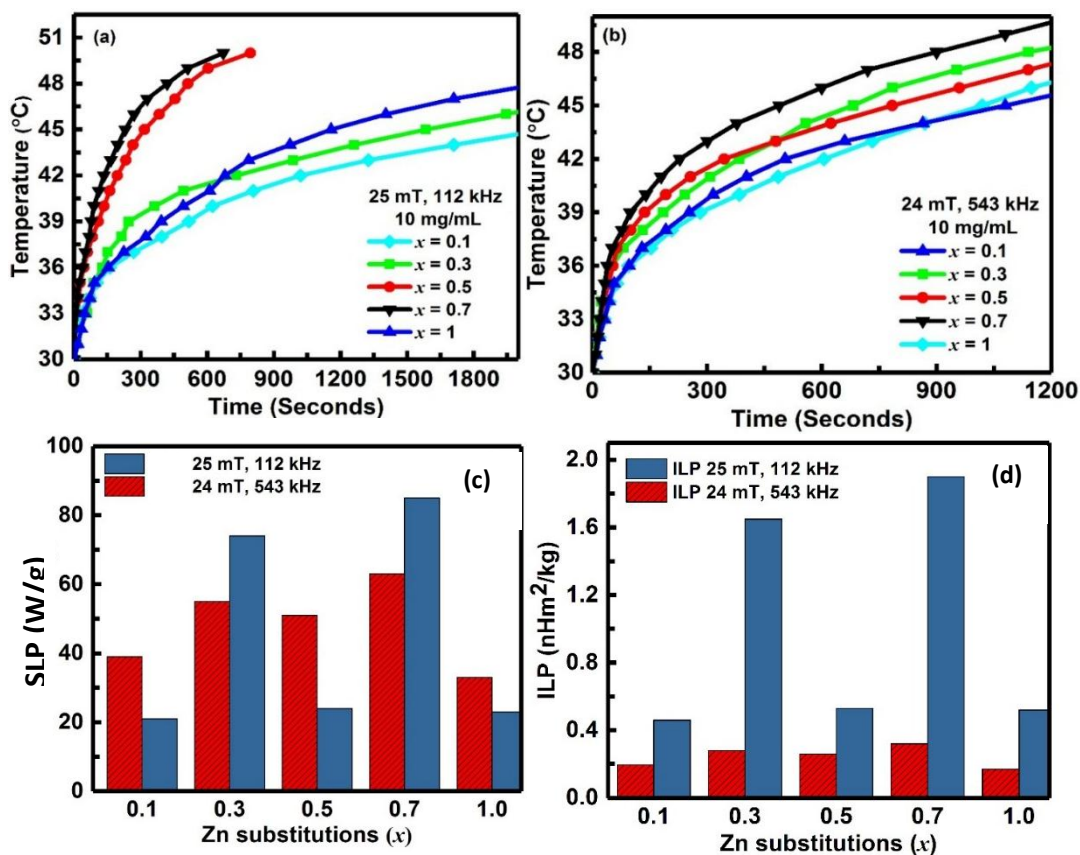

Figure 4.8: (a) and (b) Temperature rise dependent on magnetic fluid hyperthermia curves for the concentration of 10 mg/mL at two fields, (c) magnitude of the SLP and (d) ILP for all the ferrofluids Zn$_x$Fe$_{3-x}$C (x = 0.1, 0.3, 0.5, 0.7 and 1) at both the fields.

It has been well addressed in the literature that heating behavior of MNPs in the AC magnetic field does not depend on their M_S values alone. It also gets influenced by the initial susceptibility of MNPs, their morphology as well as on the strength of the applied magnetic fields. Thus, the improved heating efficiency with increased Zn content in Fe$_3$C may be

attributed to their shape anisotropy because it modifies from spherical to cuboidal shape (Figs. 4.3 a and 4.4 a). The specific loss power (SLP), the index of heating performance of MNP_S was also calculated at both the fields and are shown in Fig 4.8 (c). The magnitude of SLP at 25 mT field was 21, 74, 24, 85, and 23 W/g for the samples $x = 0.1, 0.3, 0.5, 0.7$ and 1 respectively. The maximum SLP value was 85 W/g for $x = 0.7$ sample and the lowest value was 21 W/g for $x = 0.1$. Similarly, at 24 mT field, the SLP value was 39, 55, 51, 63 and 33 W/g for the ferrofluids of samples $x = 0.1, 0.3, 0.5, 0.7$ and 1 respectively. It was noticed that the SLP value was optimum for $x = 0.7$ sample at both the fields. The SLP values for the present samples were more than that of Co-substituted Fe_3C samples [25]. This may be attributed to the relatively higher M_S values for the present samples. The obtained SLP values were comparable with some of the reported values for iron oxide based MNPs. Fig. 4.8 (d) shows the ILP values for various ferrofluids. At 25 mT, the magnitudes of ILP values were 0.46, 1.65, 0.53, 1.9 and 0.52 nHm^2/kg for the magnetic ferrofluids of samples $x = 0.1, 0.3, 0.5, 0.7$ and 1 respectively. Here, it can be perceived that the ILP values had a similar trend as that of the SLP values. The maximum and minimum ILP values were found to be 1.9 and 0.46 nHm^2/kg for the ferrofluids of $x = 0.7$ and 0.1 respectively. On the other hand, at the field of 24 mT, the ILP values for the ferrofluids of samples $x = 0.1, 0.3,$ 0.5, 0.7 and 1 were 0.196, 0.28, 0.26, 0.32, and 0.17 nHm^2/kg respectively. At this field also, the ILP values had a comparable variation to that of the SLP values. In summary, it can be inferred that the obtained SLP and ILP values are comparable to that for magnetic iron oxide based nanomaterials [25, 39, 45].

4.2.8 *In-vitro* study

The biocompatibility of the $Zn_xFe_{3-x}C$ ($x = 0.5$ and 1) MNPs was evaluated with A549 cell lines via SRB assay and the obtained results are shown in Fig. 4.9. The figure 4.9 (a) shows the cells in the well of 96 well plate after 24 h of seeding which suggests their normal growth. Similarly Fig. 4.9 (b), represents the cells treated with $x = 0.5$ sample of concentration 1 mg/mL after 24 h. The dark particles observed in the micrograph (Fig. 4.9 b) are MNPs which did not affect the growth of the cells. The cell viability of the ferrofluids of $x = 0.5$ and 1 samples were done at different concentrations of MNPs such as 0.1, 0.5, 1, 1.5, 2, 2.5 and 3 mg/ml with media (as shown in Fig. 4.9 c). After 24 h of treatment, the % cell viability for $x = 0.5$ sample was 99 % at 0.1 mg/mL and decreased to ~ 90 % at 2 mg/mL concentration. Further, it decreased to 86 and 82 % at 2.5 and 3 mg/mL respectively. Similarly, after 24 h, for $x = 1$ sample, the viability was observed to be 99 and 89 % at the concentrations of 1 and 2 mg/mL respectively. For the same sample, the viability reduced to 86 and 84 % at 2.5 and 3 mg/mL of MNPs respectively. There was no significant decrease in the cell viability even after 48 h of treatment at lower concentrations (i.e. up to 2 mg/mL of MNPs). For example, the samples $x = 0.5$ and 1 had viability around 98 % at the concentration of 0.1 mg/mL. It decreased to 88 % for the two samples at a concentration of 2 mg/mL. However, at highest concentration i.e. 3 mg/mL, for $x = 0.5$ and 1 samples, the viability decreased to 84 and 82 % respectively. The cell morphology was also observed by Fluorescence microscopy which is shown in Fig. 4.9 (d). The fluorescence micrograph of the A549 cells was taken after the treatment with MNPs ($x = 0.5$) at a concentration of 1 mg/mL

for 24 h. The micrograph suggests that the cells had normal growth and MNPs were not causing any mechanical or chemical damages to them.
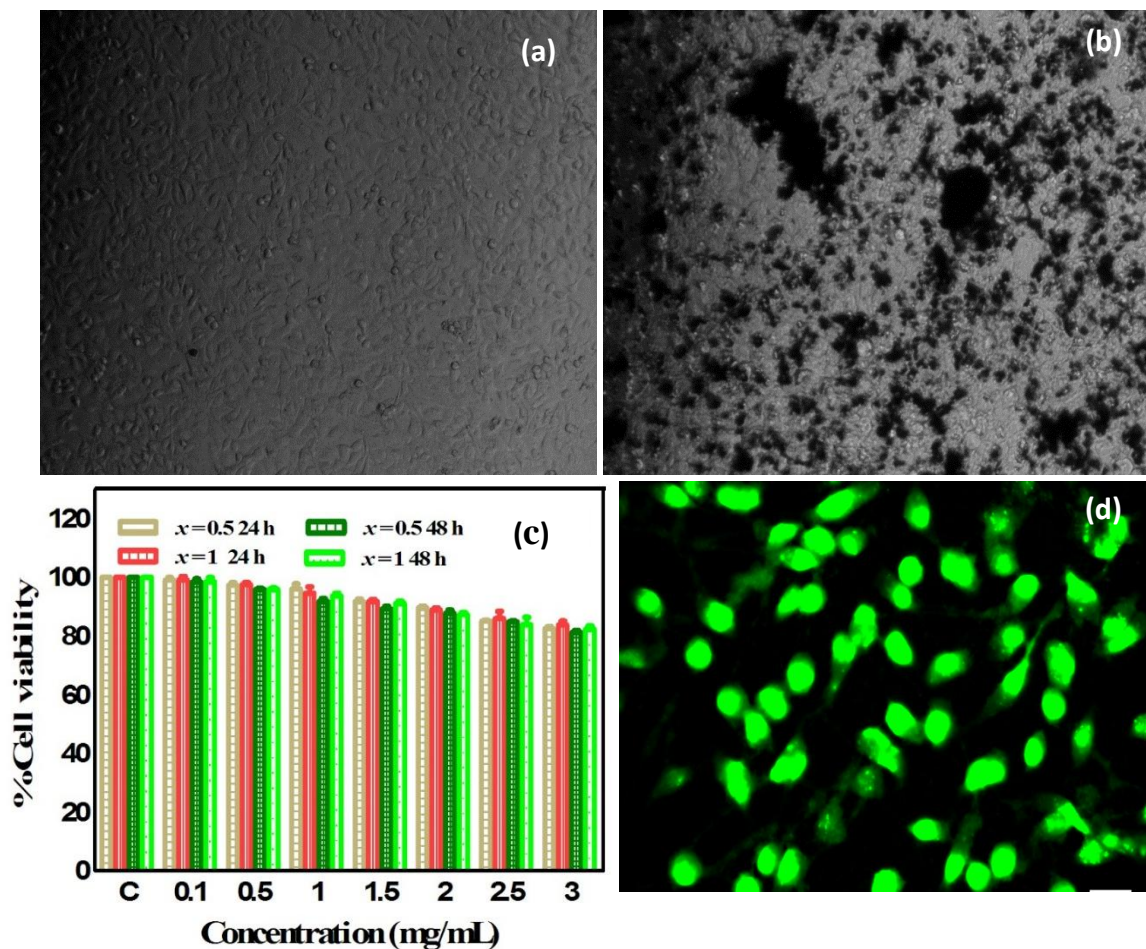

Figure 4.9: Compatibility of $Zn_xFe_{3-x}C$ nanoparticles with A549 lung cancer cell lines. a) control cells morphology after 24 h incubation period b) cells were treated with the MNP$_S$ ($x = 0.5$) of 1 mg/ml concentration for 24 h c) % cell viability of the F127 functionalized samples $x = 0.5$ and 1, with varying concentrations (0.1, 0.5, 1, 1.5, 2, 2.5 and 3 mg/mL) at diffrerent incubation period d) Fluorescence imaging after stained with acridine orange.

4.3 Conclusions

In summary, the successful synthesis of $Zn_xFe_{3-x}C$ MNP$_S$ has been done using the sol-gel assisted technique. The XRD, electron diffraction and Mössbauer spectroscopy have confirmed the single-phase nature for all the samples. From the TEM analysis, it was found that the particles were in the nanometric range (10-40 nm). XPS spectra suggest the oxidation states for corresponding elements (e.g. Fe, Zn and C) in the samples. Magnetic properties measurement shows only a slight reduction in magnetization values with increased Zn substitutions. The MHT experiments indicated that the heating efficacy of these samples at two different AC fields was suitable for magnetic hyperthermia application. The samples ($x = 0.5$ and 1) have shown around 88 % cells viability at a concentration of 2 mg/mL after 48 h of treatment. Hence, these materials may be evaluated by *in-vivo* analysis for the applications as magnetic biomaterials.